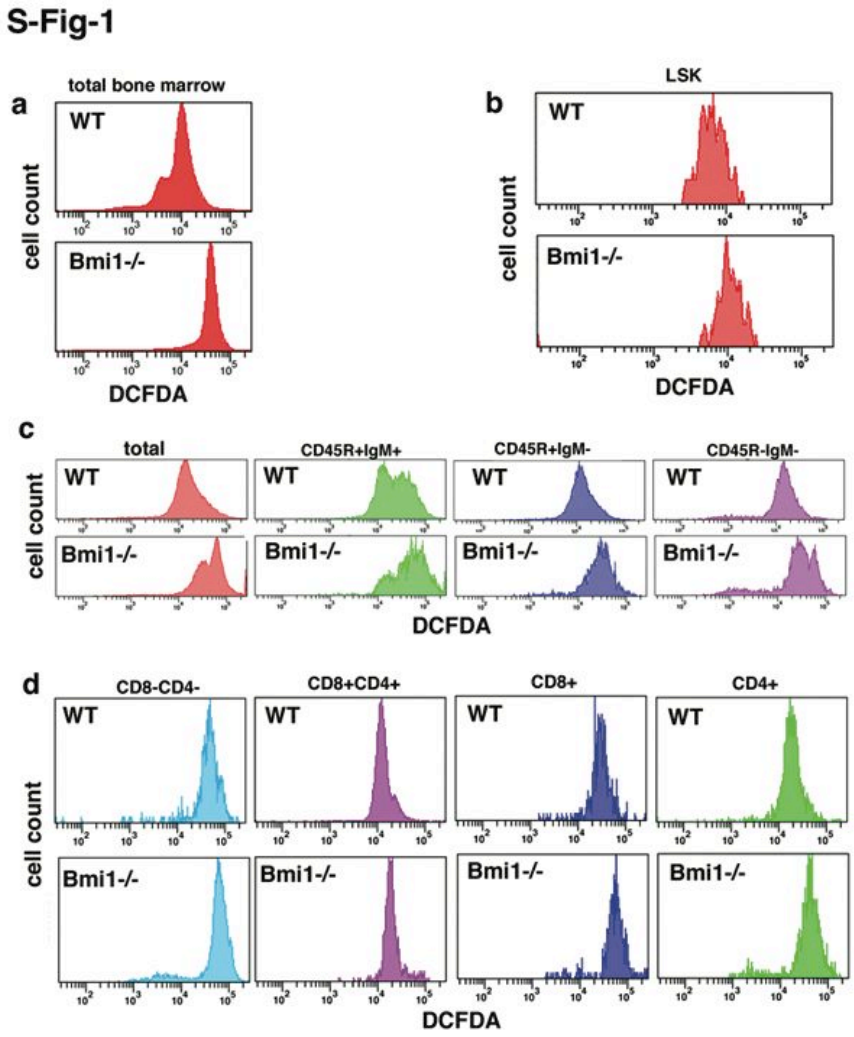

Figure 1: ROS levels are elevated in various cell types obtained from Bmi1-/- mice. **a**. ROS levels in total bone marrow cells isolated from WT or Bmi1-/- mice. **b**. ROS levels in purified LSK cells. c. ROS determinations in either total splenocytes obtained from WT or Bmi1-/- mice or from various sub-fractions of splenocytes. **d**. Levels of ROS in various purified subpopulations of thymocytes obtained from WT or Bmi1-/- mice.

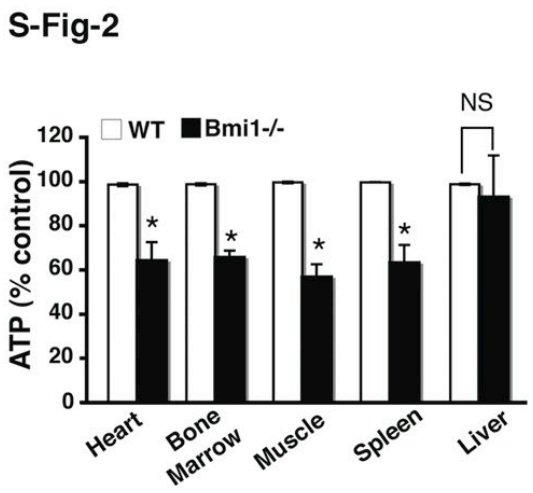

Figure 2: Measurement of basal ATP levels in WT or Bmi1-/- mouse tissues. ATP was assessed per mg of protein. Values are normalized in each tissue type to the levels observed in the wild type animals (100%). Measurements were made in triplicate and are the mean +/- SD of 4 animals per group. * $p<0.005$.

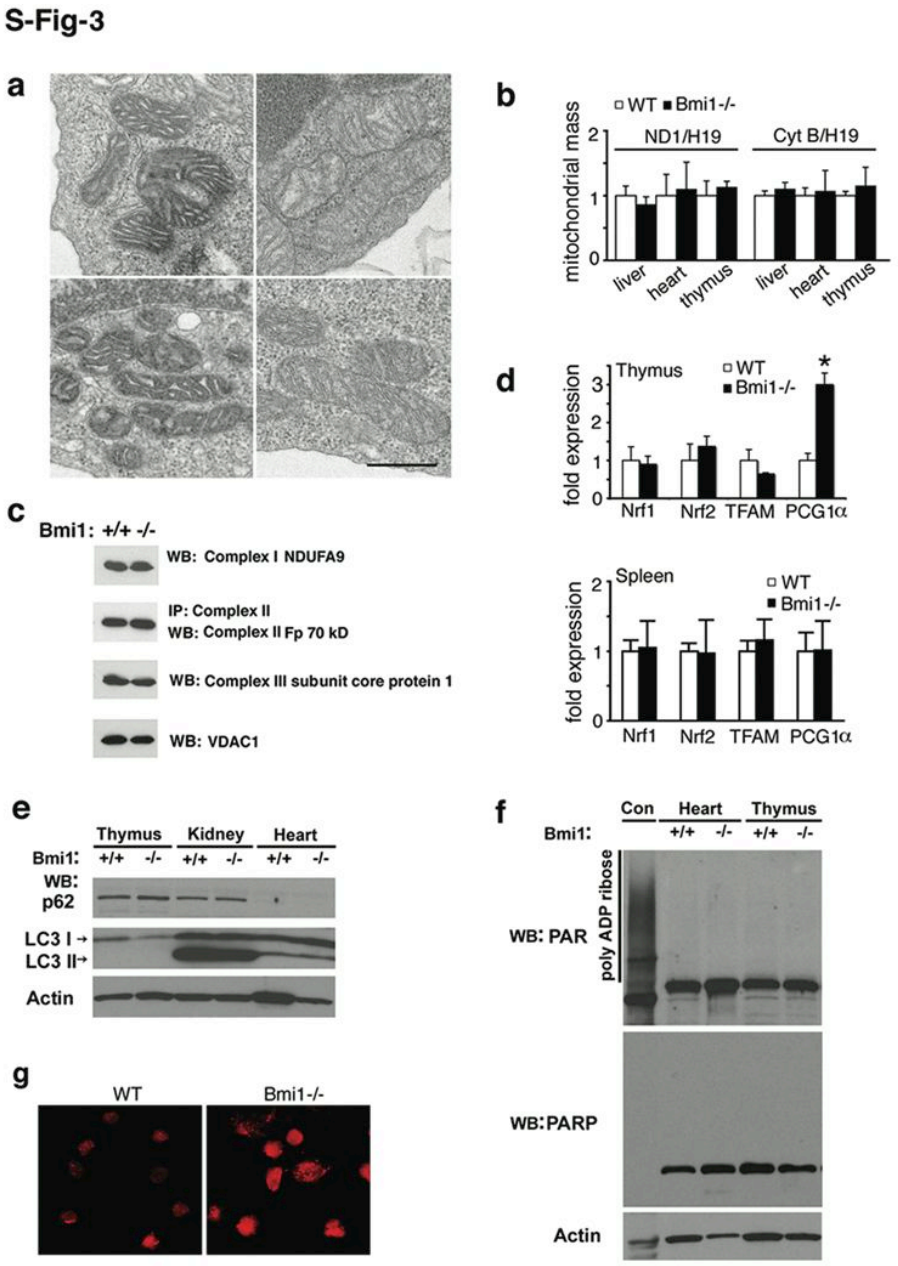

Figure 3: Comparison of various mitochondrial parameters in WT (+/+) and Bmi1-/- cells and tissues. **a**. Electron micrographs of WT (upper panels) and Bmi1-/- (lower panel) thymocytes (bar=500nm). In both genotypes, we observed a range of mitochondrial morphologies which may relate to differences in thymocyte maturation. Nonetheless, there was no discernable qualitative difference observed between WT and Bmi1-/- cells with respect to overall mitochondrial

morphology. **b**. Mitochondrial mass as determined by the ratio of mitochondrial to nuclear genomes in various tissues from WT and Bmi1-/- mice. WT levels of mitochondrial to nuclear genomes was set at '1' for each tissue. Two different mitochondrial encoded genes were used including ND1 and CytB. In both cases, we observed no evidence for increased or decreased mitochondrial mass in knockout tissues. **c**. Expression of various mitochondrial proteins isolated from the heart of wild type and Bmi1-/- mice are compared. Western blotting of VDAC1 and specific components of the electron transport chain were performed. Equal amounts of mitochondrial protein lysate (50 μg) were loaded on an SDS-PAGE gel and the specific expression of subunit 9 of Complex I (NDUFA9), a 70kD component of Complex II, subunit core protein 1 of Complex III and VDAC1 were determined in wild type and Bmi1-/- mitochondria. **d**. Expression of four genes linked to mitochondrial biogenesis were assessed in both the thymus and spleen of WT and Bmi1-/- mice using quantitative RT-PCR analysis (n=3 for each genotype). The only observed difference that was of statistical significance was the expression of PGC-1α in the thymus. This increase was not seen in other tissues and is of unclear significance. **e.** Assessment of autophagy/mitophagy in WT (+/+) and Bmi1-/- tissues using a marker of autophagosome formation (ratio of LC3-I to LC3-II) and autophagic flux (p62 levels). While levels of autophagy showed marked tissue specific differences, within a given tissue, no differences in autophagy were seen between WT and Bmi1-/- mice. **f**. Assessment of PARP activity in WT (+/+) and Bmi1-/- tissues. Two related measurements for PARP activity were employed including assessment with an antibody directed against poly ADP-ribose moieties (WB:PAR) or directly against the enzyme Poly ADP-Ribose Polymerase-1 (WB:PARP). A control lysate (Con) of previously ADP-ribosylated protein was supplied by the manufacturer (Trevigen). **g**. Representative images of thymocytes loaded with the mitochondrial superoxide fluorphore MitoSox Red and imaged by confocal microscopy.

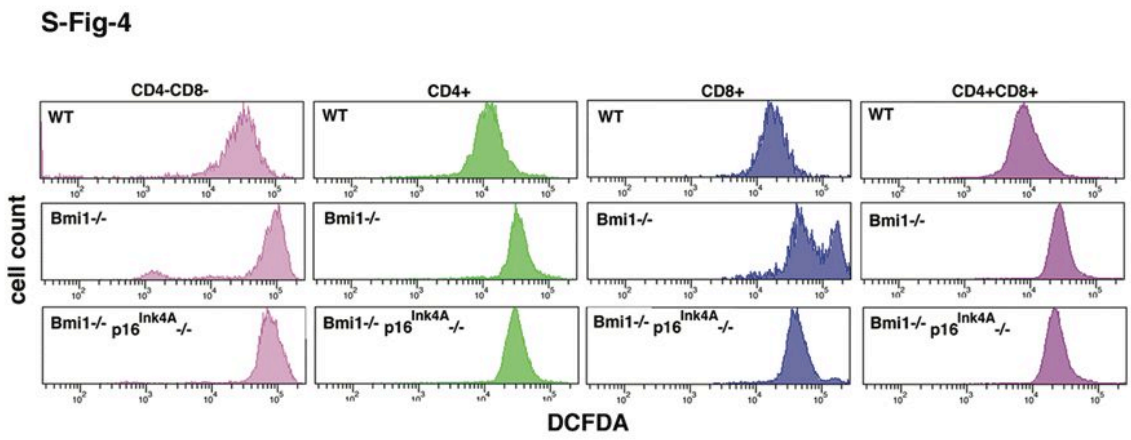

Figure 4: ROS levels in thymocytes are not effected by *p16*^{Ink4a} deletion. Analysis of ROS levels in various sub-populations of double negative, single positive and double positive (CD4+/CD8+) thymocytes obtained from WT, Bmi1 and combined Bmi1/ *p16*^{Ink4a} deleted mice. The deletion of *p16*^{Ink4a} does not alter levels of ROS induced by Bmi1 deletion.

S-Fig-5

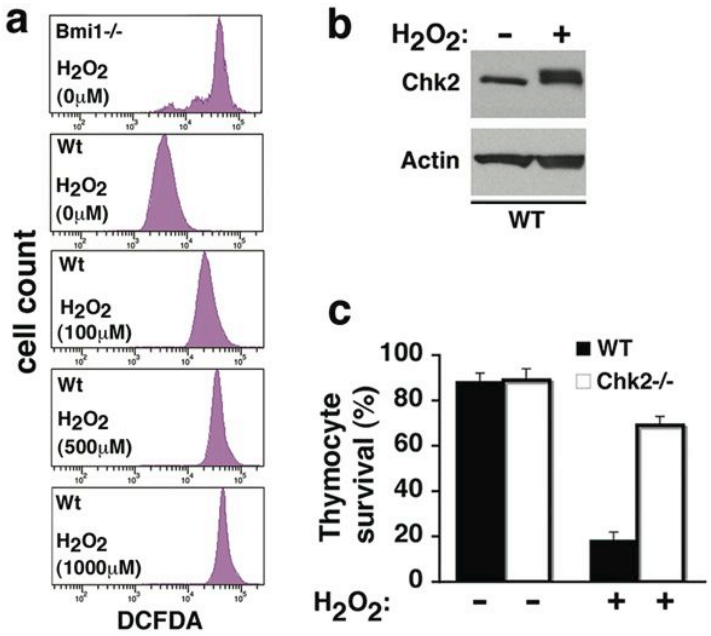

Figure 5: Activation of Chk2 in thymocytes is stimulated by oxidative stress. **a**. Analysis of ROS levels in WT thymocytes after exogenous hydrogen peroxide exposure (100-1000 μM). For comparison, the basal level of ROS seen in Bmi1-/- thymocytes is shown. **b**. Chk2 is activated in wild type thymocytes when assessed 30 minutes after exposure to 500 μM exogenous hydrogen peroxide. **c**. Hydrogen peroxide treatment (100 μM for 30 minutes) induces significant loss of cell viability at 24 hours in wild type thymocytes while Chk2-/- thymocytes appear largely protected from this same oxidative stress.

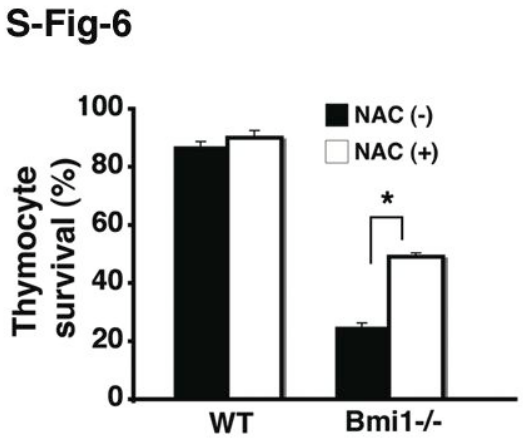

Figure 6: Primary thymocyte cultures were isolated from wild type or Bmi1-/- mice and directly placed into standard tissue culture medium and cellular viability assessed 24 hours later. Thymocytes lacking Bmi1 survive poorly under these conditions and their survival can be enhanced by incubation with the peroxide scavenger N-acetylcysteine (NAC, 500μM: *$p<0.001$).

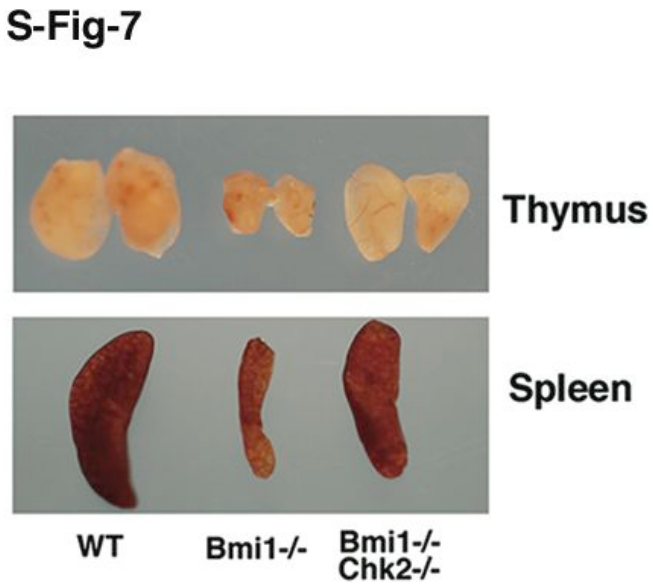

Figure 7: Chk2 deletion restores the overall size of the thymus and spleen in Bmi1-/- mice. Representative thymuses and spleens harvested from 2 months old mice. The overall thymus and spleen size of Bmi1 -/- mice that survived to this age were significantly smaller than wild type mice and this phenotype was mitigated by concurrent Chk2 deletion.

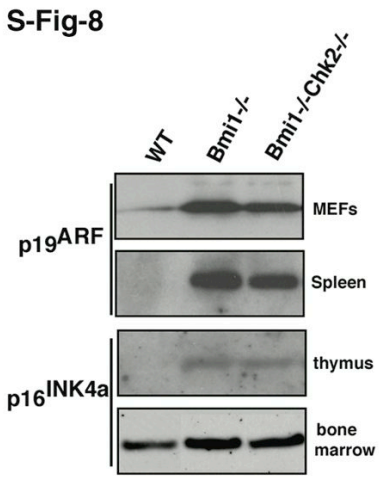

Figure 8: Chk2 deletion does not alter protein expression of $p19^{ARF}$ or $p16^{Ink4a}$. Representative Western blot analysis of either $p19^{ARF}$ or $p16^{Ink4a}$ in mouse embryonic fibroblasts, splenocytes, thymocytes or total bone marrow cells.

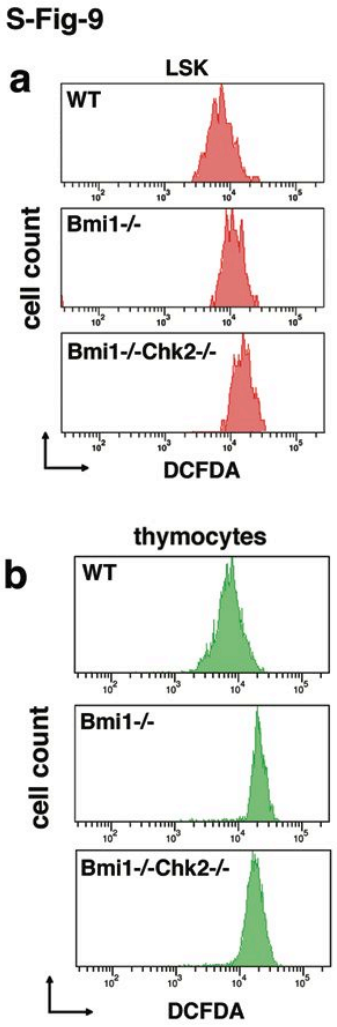

Figure 9: Deletion of Chk2 does not alter levels of ROS in mice deficient in Bmi1. Levels of ROS were analyzed in **a**. LSK cells purified from WT, Bmi1-/- or combined Bmi1/Chk2 deficient bone marrow. **b.** thymocytes obtained from the indicated genotypes. ROS levels were similarly elevated in Bmi1 deficient cells irrespective of Chk2 status. These results are consistent with Chk2 activation being downstream of the rise in ROS levels. We interpret these data as not indicating that ROS levels are irrelevant. Rather we believe these observations indicate that a rise in ROS triggers specific rather than random pathways in cells. Our data suggests the DDR is one such redox-specific pathway. As such, in this context ROS can be viewed as acting as signaling molecules and the DDR represents a redox-dependent pathway mediating their effects[6].

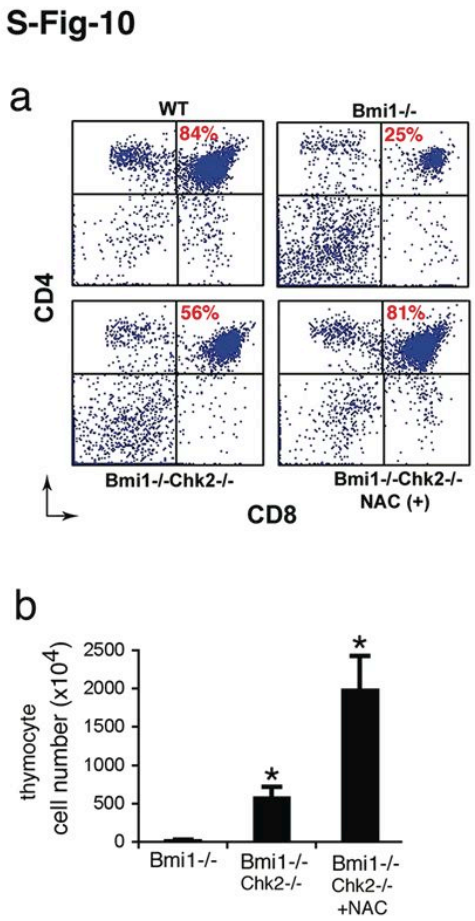

Figure 10: Antioxidant treatment can augment the rescue observed by Chk2 deletion in Bmi1-/- thymocytes. **a**. Representative level of thymocyte maturation observed in WT mice, Bmi1-/- mice, combined Bmi1/Chk2 deleted mice and antioxidant treated Bmi1/Chk2 deleted mice. The addition of NAC appears to increase thymocyte maturation even in the setting of Chk2 deletion suggesting the potential for ROS-mediated pathways that are DDR independent. **b**. A similar analysis for thymocyte number.

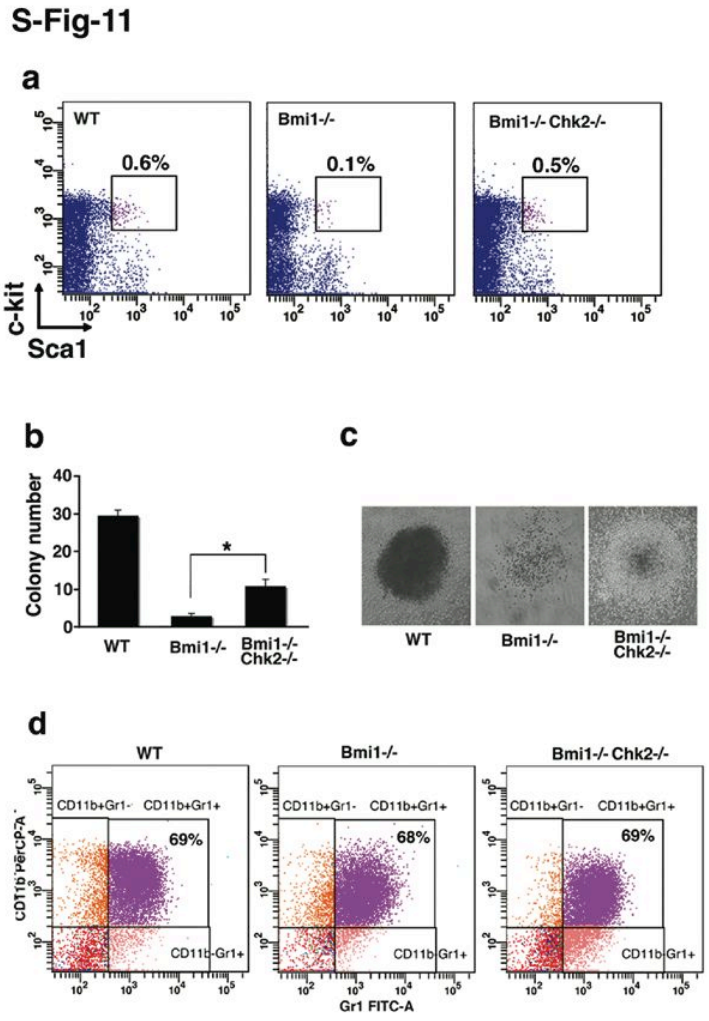

Figure 11: The *in vitro* impairment in colony formation observed in Bmi1 progenitor cells can be rescued by deletion of Chk2. **a**. Typical bone marrow analysis of LSK frequency using Lin- cells obtained from WT, Bmi1-/- or combined Bmi1/Chk2 deficient mice. **b.** *In vitro* colony assay (granulocyte-monocyte differentiation media) using equal numbers of purified bone marrow cells obtained from wild type, Bmi1-/- and combined Bmi1/Chk2 deficient mice. **c.** Observed representative *in vitro* methylcellulose colony morphology demonstrating that Bmi1-/- LSK cells produce fewer and less well formed colonies. **d**. Representative analysis of the granulocyte-macrophage colony composition demonstrating that although the frequency is different, the ultimate *in vitro* maturation is similar between the three genotypes.

S-Fig-12

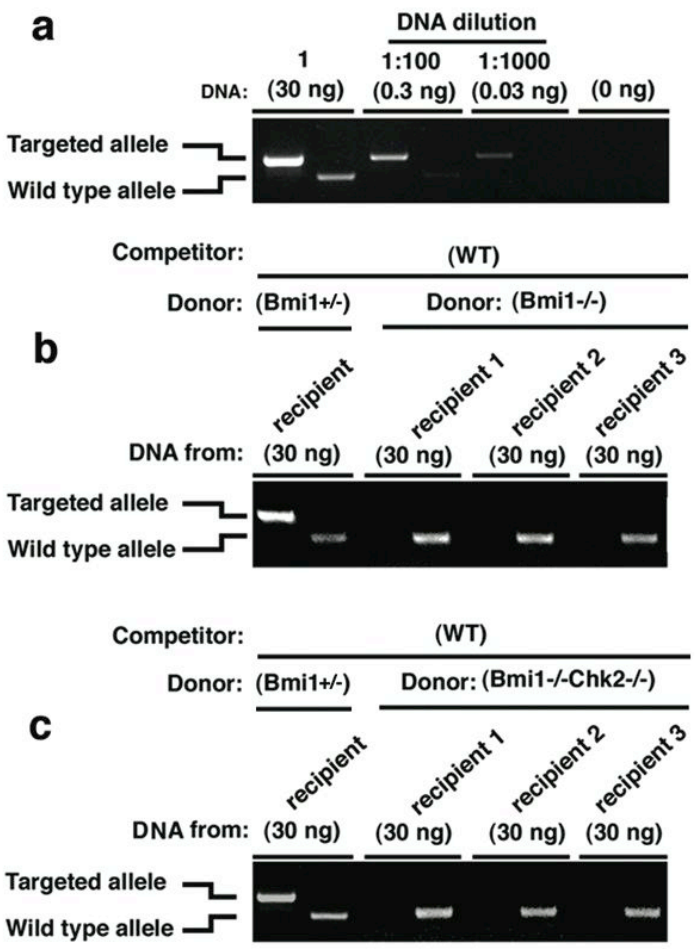

Figure 12: PCR based analysis of long term competitive repopulation. **a.** Analysis of both the wild type and targeted Bmi1 allele following PCR of genomic DNA isolated from circulating cells of a Bmi1+/- mouse. The targeted allele runs at a slighter slower mobility than the wild type allele. Using serial dilutions, the targeted allele is still discernable at a 1:1000 dilution of the original DNA. **b.** PCR of 30 ng of genomic DNA template isolated 4 months after transplantation in competitive repopulation experiments with either a Bmi1-/- or Bmi1+/- mouse as a donor and wild type bone marrow as a competitor. Shown are a single recipient from the Bmi1+/- donor and three separate transplant recipients from the Bmi1-/- donor. These results demonstrate the absence of amplification of the targeted Bmi1 allele when Bmi1-/- mice serve as the donor and

when using DNA (30 ng) isolated from circulating cells as a template. As such, these results are consistent with previous observations demonstrating the absence of LT-HSC self-renewal capacity in Bmi1-/- marrow. **c.** Similar analysis from one recipient who received Bmi1+/- marrow as the donor cell population and 3 other transplanted recipients that received combined Bmi1/Chk2 deleted donor cells. All recipients also received wild type bone marrow as a competitor. Again, there was no detected amplification of the targeted Bmi1 allele when Bmi1/Chk2 deleted marrow served as the donor population. Based on the serial dilutions in panel A, the absence of detection of the targeted allele in panel B and C suggests that four months after transplantation, the frequency of cells derived from Bmi1-/- alone or combined Bmi1/Chk2 deleted stem cells was estimated to be at or below 1 in a 1000 circulating cells.

S-Fig-13

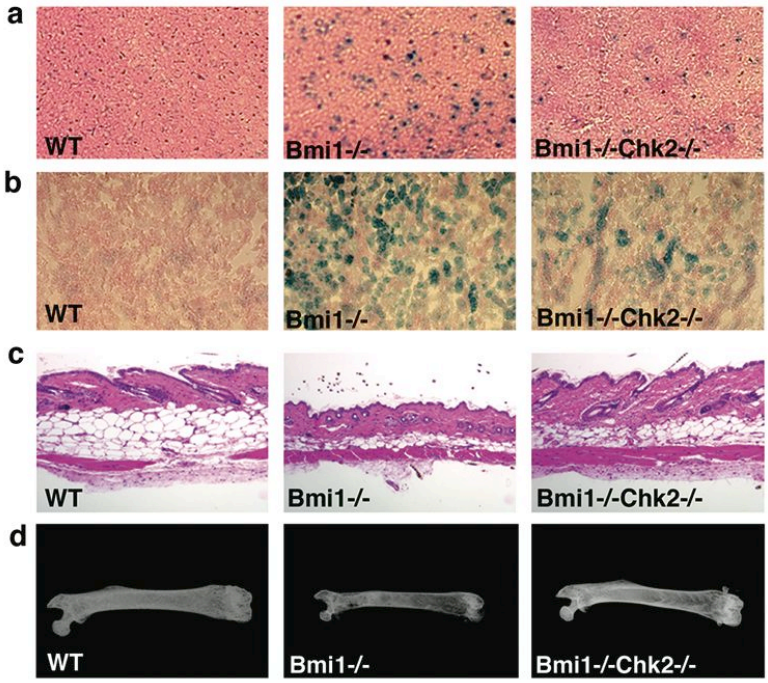

Figure 13: Bmi1-/- mice exhibit evidence of increased in vivo senescence and changes consistent with accelerated ageing that are mitigated by Chk2 deletion. Aged-matched ten week old tissues were assessed for senescence using the SA β-gal assay. Representative tissue analysis from **a**. brain and **b.** kidney demonstrate increased SA β-gal staining in the Bmi1-/- mice. In addition, we noted changes consistent with accelerated ageing including **c**. reduced skin thickness and decreased subcutaneous adiposity and **d**. reduced bone density in the femur of 10 week old Bmi1-/- mice. These abnormalities are reversed in part by concomitant Chk2 deletion.

Supplemental Methods and Materials:

Analysis of the DDR pathway:

For assessment of DDR pathway activation, we employed freshly isolated thymocytes from 4 weeks old Bmi1+/+ and Bmi1-/- mice treated with and without NAC for one week. CytoSpin cells were fixed with 4% paraformaldehyde and permeabilized with 0.1% Triton X-100. Cells were incubated for 1 hour in blocking buffer composed of 3% BSA in PBS and then incubated with anti-53BP1 (Novus, 1: 1000) overnight at 4 ºC. Percentage positive staining was calculated by counting >100 random nuclei from three pairs of pooled thymocytes.

For detection of Chk2 activation, cells and tissues were homogenized in ice-cold lysis buffer (50 mM Tris·HCl, 1% Nonidet P-40, 0.5% Na deoxycholate, 150 mM NaCl,) supplemented with protease inhibitor cocktail (complete mini tablet, Roche) and phosphatase inhibitor (Pierce). Equal amount of proteins were separated by SDS-PAGE. Western blot analysis was done according to standard methods using the mouse monoclonal anti-Chk2 antibody (BD Transduction Laboratories) followed by enhanced chemiluminescence detection (Amersham).

In vivo analysis

Senescence associated β-galactosidase staining (SA-βgal) of various tissues was performed essentially as initially described[1]. Tissues were processed for routine analysis after fixation in 4% paraformaldehyde. Bone density was assessed by an X-ray dose of 15

kV for 100 seconds using a Faxitron X-ray apparatus. The *in vivo* determination of thymocyte maturation was performed as previously described[2]. TUNEL assay was performed using the ApopTag Peroxidase In Situ Detection Kit (Chemicon) according to the manufacturer's recommendation.

Mitochondrial and viability assays

For the detection of relative protein abundance we employed antibodies against mitochondrial proteins included the Complex I subunit NDUFA9 (Abcam), the Complex II 70 kDa Fp subunit , the Complex III core 1 subunit (both from Mitoscience) or VDAC1/porin (Invitrogen). Mitochondrial NADH levels were assessed by endogenous cellular fluorescence measured at an excitation of 350 nm and an emission of 440 nm. This signal has been previously shown to correlate with NADH levels[3]. For electron micrograph assessment of mitochondrial morphology, thymocyte cell pellets were immediately fixed in a mixture of 2.5% glutaraldehyde and 1% paraformaldehyde in 0.12M sodium cacodylate buffer, pH 7.3. After fixation, the pellets were postfixed with 1% osmium tetroxide, stained en bloc with 1% uranyl acetate, dehydrated and embedded in Embed 812 resin by standard techniques. Thin sections were stained with uranyl acetate and lead citrate. Images were acquired with a JEM 1200EX transmission electron microscope equipped with an AMT 6 megapixel digital camera.

Determination of mitochondrial mass was performed by analyzing the ratio of mitochondrial DNA to nuclear DNA as previously described[4]. In brief, the abundance of the mitochondrial encoded gene ND1 or CytB was compared to the abundance of the

nuclear gene H19. For analysis of the genes regulating mitochondrial biogenesis we analyzed expression of NRF1, NRF2, TFAM and PGC-1α using the following primer pairs.

Primers	Orientation	Sequence (5' to 3')
Nrf1	sense	GAGTCAACGGATTTGGTCGT
Nrf1	antisense	TTGATTTTGGAGGGATCTCG
Nrf-2a		CTCCCGCTACACCGACTAC
Nrf-2a		TCTGACCATTGTTTCCTGTTCTG
TFAM		CCGAAGTGTTTTTCCAGCAT
TFAM		CAGGGCTGCAATTTTCCTAA
PGC-1α		CGG AAA TCA TAT CCA ACC AG
PGC-1α		TGA GGA CCG CTA GCA AGT TTG

For analysis of autophagy/mitophagy, we measured LC3-I to LC3-II ratios to assess autophagosome formation and monitored p62 levels to assess autophagic flux[5]. The specific antibodies employed included p62 (Progen) and LC3 (Sigma). Activation of PARP dependent pathways included assessment of the level of poly-ADP ribosylated proteins using and anti-PAR antibody (Trevigen) as well as and antibody directed against PARP (Enzo Life Sciences). MitoSox fluorescence (Invitrogen) was assessed by FACS scan analysis (LSRII instrument) or via confocal imaging according to the manufacturer's recommendations.

For cell viability assays, thymocytes and splenocytes were freshly isolated from 6-8 week old mice and were plated at an initial density of $1x10^6$ cells/ml in Dulbecco Modified Essential Medium (DMEM) supplemented with 10% fetal bovine serum.

Viability was determined 24 hours later using trypan blue exclusion and by counting at least 300 random cells per condition. To rescue thymoctye viability in vitro, where indicated, N-acetylcysteine (Sigma) was added at a concentration of 500 μM.

Gene expression analysis

Analysis of gene expression was performed with a MxP3005P real-time PCR system (Stratagene) using SYBR Green PCR Mastermix (Applied Biosystems) according to the manufacturer's instruction. The following is a list of the primers employed for $p16^{Ink4a}$, $p19^{Arf}$, dual oxidase 1 (Duox1), dual oxidase 2 (Duox2), lactoperoxidase (Lpo), cysteine dioxygenase (CDO1), arachidonate 5-lipoxygenase (Alox5), arachidonate 15-lipoxygenase (Alox15), cytochrome p450 family 24 (Cyp24A1), cytochrome p450 family 26 (Cyp26A1), BCL2/adenovirus E1B 19kDa interacting protein 3-like (Bnip3L),BH3 only pro-apoptotic (Noxa), glyceraldehyde-3-phosphate dehydrogenase (Gapdh).

List of real time RT-PCR primers:

Primers	Orientation	Sequence (5' to 3')
$p16^{Ink4a}$	sense	GTACCCCGATTCAGGTGATG
$p16^{Ink4a}$	antisense	GGAGAAGGTAGTGGGGTCCT
$p19^{Arf}$		CCCACTCCAAGAGAGGTTTT
$p19^{Arf}$:		ATGTTCACGAAAGCCAGAGC
Duox1		CTGTACCTCGATGGACCGTTTGGAGA
Duox1		AGTCCTTGTCACCCAGATGAAGTAGA
Duox2		TCCATCCTCAAAGACCTGGTCTTCA
Duox2		CTCAGCCAGCTGAGTAATGTAGATGT
Lpo		CTGGACCAGAAGAGATCCATG
Lpo		TCACCAGGTGGGAACATGATGG

CDO1	GTGGATCAAGGAAATGGGA’
CDO1	CTTGATCATCTCGTTGGA
Alox5	CATGTTACCGCTGGATCA’
Alox5	CCACTCCATCCATCTATACTG
Alox15	GACTTGGCTGAGCGAGGACT
Alox15	CTTGACACCAGCTCTGCA
Cyp24A1	GATGAGCACATTTGGGAAGATG
Cyp24A1	GCACCAGGCTGCTGGGAATATC
Cyp26A1	GTGCGCACCATCCTGGGCGCTG
Cyp26A1	CTGCTCCAGACAACTGCTGACTTC
Bnip3L	CTGAGCACACCTTCTGCCAGC
Bnip3L	TAGGGATCATGCTTACAATAGGTC
Noxa	GAACGCGCCAGTGAACCCAA
Noxa	CTTTGTCTCCAATCCTCCGG
Gapdh	ATGACATCAAGAAGGTGGTGAAG
Gapdh	TCCTTGGAGGCCATGTAGG

Supplemental References:

1. Dimri, G.P., *et al.* A biomarker that identifies senescent human cells in culture and in aging skin in vivo. *Proc Natl Acad Sci U S A* **92**, 9363-9367 (1995).

2. Jacobs, J.J., Kieboom, K., Marino, S., DePinho, R.A. & van Lohuizen, M. The oncogene and Polycomb-group gene bmi-1 regulates cell proliferation and senescence through the ink4a locus. *Nature* **397**, 164-168 (1999).

3. Combs, C.A. & Balaban, R.S. Enzyme-dependent fluorescence recovery after photobleaching of NADH: in vivo and in vitro applications to the study of enzyme kinetics. *Methods Enzymol* **385**, 257-286 (2004).

4. Pagel-Langenickel, I.*, et al.* PGC-1alpha integrates insulin signaling, mitochondrial regulation, and bioenergetic function in skeletal muscle. *J Biol Chem* **283**, 22464-22472 (2008).

5. Klionsky, D.J.*, et al.* Guidelines for the use and interpretation of assays for monitoring autophagy in higher eukaryotes. *Autophagy* **4**, 151-175 (2008).

6. Finkel, T. & Holbrook, N.J. Oxidants, oxidative stress and the biology of ageing. *Nature* **408**, 239-247 (2000).